ELSEVIER

Organic Electronics 3 (2002) 81–88

Organic Electronics

www.elsevier.com/locate/orgel

The morphological dependence of charge transport in a soluble luminescent conjugated polymer

Czek Haan Tan [a], Anto Regis Inigo [a], Wunshain Fann [a,*], Pei-Kuen Wei [b], Gung-Yeong Perng [c], Shaw-An Chen [c]

[a] *Institute of Atomic and Molecular Sciences, Academia Sinica and Department of Physics, National Taiwan University, P.O. Box 23-166, Taipei, Taiwan, ROC*

[b] *Institute of Applied Science and Engineering, Academia Sinica, Taipei 115, Taiwan, ROC*

[c] *Department of Chemical Engineering, National Tsing Hwa University, Hsinchu 300, Taiwan, ROC*

Abstract

Charge transport in poly[2-methoxy-5-(2′-ethyl-hexyloxy)-1,4-phenylene vinylene] is studied by employing the time-of-flight technique. Film morphology plays a key role in determining the charge transport properties. Samples prepared from toluene feature non-dispersive transport. However, after thermal annealing, charge transport is no longer non-dispersive and hole mobility drops for about one order of magnitude. Near-field scanning optical microscope images show that annealing enhanced film inhomogeneity. We propose that the inhomogeneity is responsible for the changes in the transport properties.

PACS®: 23.23.+x; 56.65.Dy

Keywords: MEH-PPV; Time-of-flight; Morphology; Near-field optical microscopy; Hole mobility; Luminent conjugated polymers

1. Introduction

Conjugated polymers have found great opportunity in the large area display technology due to the advantage of easy processing and mechanical flexibility [1]. An ongoing research interest has been directed towards the performance optimization of polymer light-emitting diodes (PLEDs). An interesting way to achieve the goal is that of heat treatments on the PLED device [2,3]. It was found that under appropriate thermal annealing conditions, properties such as the I–V and L–V characteristics, as well as the luminescence quantum efficiency can be optimized. Depending on the procedures of heat treatment, film morphology and the polymer/electrode interfacial properties can be altered which brings about an enhancement of the device performance. In addition, comparative studies by Nguyen et al. [4] showed that the choice of solvents can also have a profound impact on film morphology, and hence the performance of poly[2-methoxy-5-(2′-ethyl-hexyloxy)-1,4-phenylene vinylene] (MEH-PPV)-based PLEDs. Their results have revealed that different polymer conformations can be produced in the solution phase through proper selection of solvents [5]. Moreover, the memory of chain conformation and the extent

* Corresponding author. Tel.: +886-2-2366-8237; fax: +886-2-2362-0200.

E-mail address: fann@gate.sinica.edu.tw (W. Fann).

1566-1199/02/$ - see front matter
PII: S1566-1199(02)00037-X

of aggregation in the solution phase could be transferred to the solid phase. This eventually results in different film morphologies which, to a certain extent, account for the variations in device performance. While these device fabrication schemes and their concomitant device behavior have been acknowledged, a clear-cut understanding of the underlying mechanism needs further clarification due to the trade-off and convolution among various factors (e.g. charge injection, transport and recombination) involved in the analyses.

Charge carrier mobility is one of the important material parameters in solid-state devices. The mobility of organic and polymeric materials have been studied, among others, by using time-of-flight (TOF) [6,7] and space-charge-limited current (SCLC) [8,9] methods. In the present study, we focus on the effects of heat treatment, viz. annealing, on the charge transport properties alone by measuring the hole mobility of MEH-PPV using TOF. TOF is a conventional method which provides information about the drift of a sheet of charge carriers in the material by which the charge carrier mobility μ can be derived from the transit time t_t according to the formula

$$\mu = \frac{L^2}{Vt_t},$$

with L sample thickness and V applied bias. This technique is employed because additional information on the microscopic origin of charge transport can be gleaned from the photocurrent transients, in contrast to direct current (dc) measurements such as SCLC. However, TOF measurements generally require thick sample with thickness > 1 μm so that charges are only generated at the front layer. With the exception of poly(9,9-dioctylfluorene) [10], ladder-type methyl substituted poly-(para-phenylene) [11] and poly-(phenylenevinylene-ether) [12], many well-known conjugated polymers including poly-(phenylenevinylene) (PPV) were found to display dispersive hole transport [13–15], in the sense that discernible kinks in the photocurrent transients are absent in the double-linear and sometimes even double-logarithmic plots. Dispersive hole transport in MEH-PPV using TOF was reported by Campbell et al. [16]. Non-dispersive hole transport in MEH-PPV has been reported in our recent work [17]. In this paper, we will show that upon thermal annealing, the non-dispersive feature in the samples from toluene solution is lost. Moreover, the hole mobilities were found to be about one order of magnitude less than the unannealed films. Based on images taken by a near-field scanning optical microscope (NSOM) and spectroscopic results, the inhomogeneity is identified as an important factor for the transport properties. Possible implications with regard to device performance will be discussed.

2. Experiment

For TOF measurements, thick films were prepared by drop-casting MEH-PPV solutions onto ITO glass slide from toluene. Glass slides were cleaned before drop-casting by treating with organic solvents in the ultrasonic bath and finally with acetone and oxygen plasma. The coated films were dried for 12 h at 50 °C under constant purge of nitrogen in order to remove the residual solvent. Annealed films were prepared by heating the samples at around 210 °C in nitrogen atmosphere for 12 h and cooled down slowly in the same environment. Subsequently the sample was placed in the vacuum chamber and 1000 Å Au films were thermally evaporated by the shadow mask procedure to yield an active area of 4 mm^2. The film thickness which ranges from 2 to 4 μm was measured by a Dektak profilometer. The drop-cast film has surface roughness ~10 nm, as measured by AFM. The hole mobilities of the samples were derived from photocurrent transients measured by a digital storage oscilloscope (Tektronix TDS 744A). The charge carriers were generated at the ITO/polymer interface by 5 ns pulses at 532 nm from a YAG laser. The samples were mounted in a temperature-controlled vacuum cryostat, and kept in the vacuum (~10^{-6} mbar) for 12 h prior to the measurements. Care has been taken to ensure that $RC \ll t_t$. To reduce perturbation on electric field, the total charges injected in to the film was kept around $0.01CV$ in all cases, where C is the struc-

ture capacitance and V is the applied bias. The intersection of asymptotes to the plateau and the declining slope of the current transient is used to determine the transit times.

Due to the sensitivity of the NSOM system, optical images could only be taken from thin films prepared by spin-casting the solution on bare glass slides. The thickness of the films is around 100 nm. The surface topography and nanometer scale absorption images were taken simultaneously using NSOM in the transmission mode. A 543 nm laser was used as the light source which was brought into the near field region by a tapered fiber. The transmitted light was collected by a lens and subsequently amplified by a PMT [18]. Photoluminescence (PL) spectra were recorded by a spectrofluorometer (Fluorolog-3 FL3-22) for both thin and thick films. In order to keep the effect of self-absorption from the optically dense thick samples to the minimal, spectra were collected in the front face geometry. Furthermore, to reduce the photooxidation effect, the incident light was excited the samples from the substrate side so that PL originates from the polymer layer closest to the substrate [20]. The unannealed and annealed drop-cast films have thickness of 3.4 and 2.3 μm, respectively. Both are too thick to record absorption spectra.

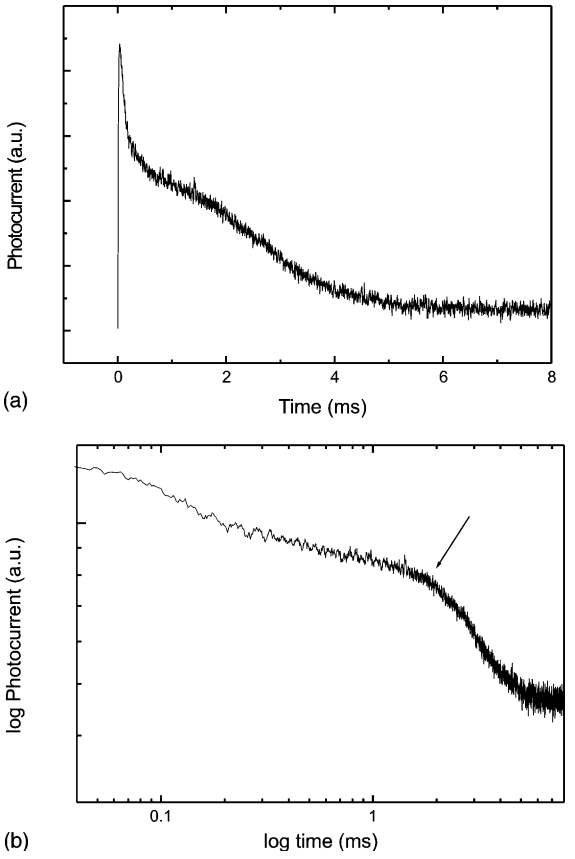

Fig. 1. The photocurrent transient of pre-annealed samples prepared from toluene in (a) linear plot, (b) log–log plot. The arrow indicates the position of transit time. The electric field is 4.4×10^4 V/cm.

3. Results and discussion

Fig. 1 shows the room temperature photocurrent transients for unannealed and annealed films prepared from toluene. Although the ideal plateau for $t < t_t$ is not observed in the TOF signal of the unannealed sample, a discernible change in the slope of photocurrent is present in linear photocurrent versus time plot, indicating non-dispersive transport [17]. However, thermal annealing has obviously removed the non-dispersive feature in toluene samples, as shown in Fig. 2. Double logarithmic plots shown in Fig. 2(b) are necessary to locate the transit times in these cases, indicating hole mobilities in these films are highly dispersive. Not only has annealing nullified the non-dispersive feature in toluene samples, but it has also reduced the hole mobility by at least one order of magnitude. For instance, the hole mobility at field 1.2×10^5 V/cm was measured to be 9.8×10^{-6} $cm^2/V\,s$, but after annealing it drops to 4.5×10^{-7} $cm^2/V\,s$ at 1.3×10^5 V/cm. Noted that the thickness of the annealed samples, 2.3 μm and unannealed samples, 3.4 μm is different. However, we have performed thickness dependent mobility studies for unannealed samples from 5 to 2 μm. There all exhibit non-dispersive transport [19]. Thus the different transport properties of annealed and unannealed samples are not due to thickness effect but are stemming from the difference in morphology.

The electric field dependence of hole mobility is presented in Fig. 3. For the unannealed samples,

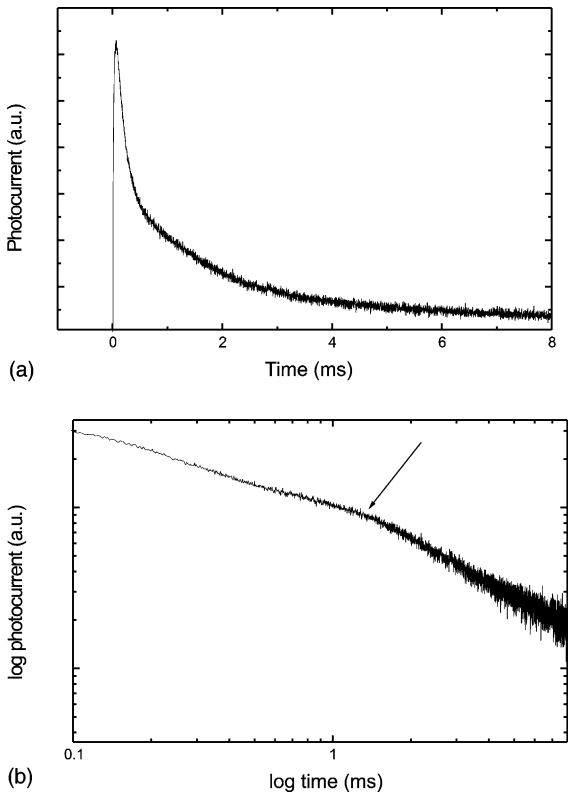

Fig. 2. The photocurrent transient of annealed samples prepared from toluene in (a) linear plot, (b) log–log plot. The arrow indicates the position of transit time. The electric field is 1.7×10^5 V/cm.

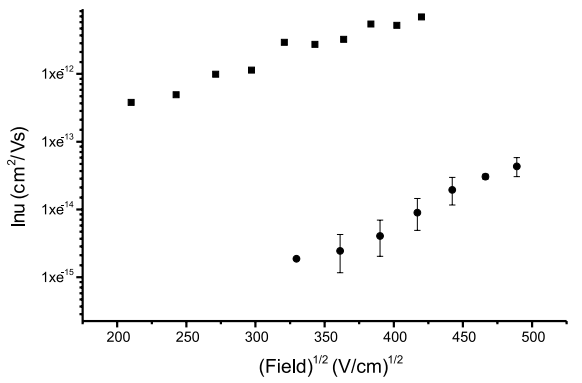

Fig. 3. The electric field dependent mobility at room temperature in pre-annealed (solid square) and annealed toluene samples (solid circle) in $\ln \mu$ versus $E^{1/2}$ plot.

the Poole–Frenkel form, generally found in a wide range of disordered materials [21–24],

$$\mu = \mu_0 \exp(\gamma \sqrt{E}),$$

is obeyed, where μ_0 and γ are sample and temperature dependent parameters. Upon annealing, the electric field dependence of hole mobility has also become more complicated. These measurements were performed at two different annealed samples because it is more difficult to allocate the transit time in dispersive transport data. For electric fields larger than 1.3×10^5 V/cm, the slope of the $\ln \mu$ versus $E^{1/2}$ plot is larger than the unannealed sample This increased of slope can be explained by Gaussian disorder transport model of Bässler and co-workers. In this model, charge transport is envisaged as a series of hopping motion across a Gaussian distribution of localized density of states (DOS) of width σ [25]. The slope increase is due to positional disorder (off-diagonal disorder). A greater positional disorder, Σ, renders the original route pre-determined by the electric field less favorable. As a consequence, other detour routes are opened with part of the path going against the field. Thus, the field tends to eliminate the faster detour route. For electric field less than 1.3×10^5 V/cm, mobility exhibit much smaller field dependent is consistent with this picture. However, the limited data points and signal to noise ratio does not allow the more thorough discussion. At larger fields, depending on the magnitude of the energetic disorder σ, this is over-compensated by the field effect on energy barriers along the field direction, and the usual Poole–Frenkel form is retained.

Previous works have indicated that polymer morphology has played significant roles in device performance. Thus optical spectroscopy and NSOM were used to study the sample morphology. The absorption and fluorescence spectra of unannealed and annealed samples are shown in Fig. 4. For the spin-cast films, the changes in shape upon annealing of the absorption spectrum (Fig. 4(a)) implies that the transport state DOS width has increased. This is consistent with the increase of the positional disorder for the annealed film, shown in Fig. 3. Both results indicate that there

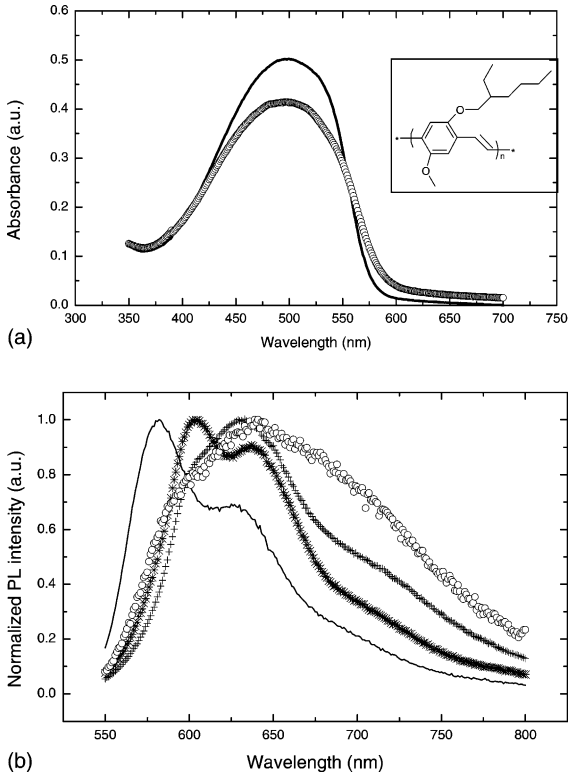

Fig. 4. (a) The absorption spectra of pre-annealed (solid line) and annealed spin-cast films (open circle). (b) PL spectra of (i) pre-annealed, spin-cast (solid line); (ii) pre-annealed, drop-cast (∗); (iii) annealed, spin-cast (open circle); and (iv) annealed, drop-cast (+) films. The inset in (a) shows the chemical structure of MEH-PPV.

has been a broadening in the distribution of interchain distances. In addition, the absorption spectrum becomes broader upon annealing, showing additional oscillator strengths at lower energies. There are more ordered or closed-packed chains with smaller energy gaps. These would effectively act as traps for holes hopping through the transport state DOS. Meanwhile, the peak emission wavelength in the PL spectrum of the annealed film is red-shifted and additional emission is found at the long wavelength regime. These indicate the formation of greater amount of aggregates due to enhanced interchain interaction upon annealing. Since PL probes the longest conjugation length/smallest energy gap chains, the red shift of the PL spectra (Fig. 4(b)) for the spin-cast films also shows that after annealing there are more deep sites which can act as carrier traps. However, the change in the relative intensity of the PL vibrational sidebands upon annealing (decrease in relative height of 0–0 compared to 1–0) indicates that the chains have a less ordered conformation, implying that most of the red shift is due to the presence of increased polarization interactions (gas-to-crystal shift) which arises from better chain packing. This is supported by the appearance of the broad excimer peak indicating intrachain interactions. The PL spectra of the drop-cast films show hardly any red shift, but do show the redistribution of the vibrational sidebands, indicating that some of the changes seen in the spin-cast films are present in the drop-cast films. However, since the PL spectrum is a combination of single-chain like emission and aggregation emission, therefore we can infer that the aggregation does not occur homogeneously across the film; some domains are more aggregated while others are less so. Investigations by Shi et al. [26] demonstrated that different film morphologies will result, depending on organic solvents, polymer solution concentrations and spin speeds employed for film preparation. Annealing is believed to provide the necessary energy so that significantly different morphologies at the initial stage converge to similar morphology eventually, an idea supported by Fig. 4(b). Therefore, although the NSOM images were taken from annealed spin-cast films, similar result from annealed drop-cast films is expected.

The topography and transmission NSOM images were taken in the unannealed and annealed samples, as shown in Fig. 5. The excitation light source is a 543 nm He–Ne laser. Before annealing, the sample assumes a flat topography and no contrast is found in the transmission image. This implies that the sample is homogeneous in the scale of 0.1 μm, which is the resolution of our NSOM. However, after the sample was annealed at 210 °C, changes in the transmission NSOM image is ensued where scattered grains of different sizes can be found. However, in terms of topographic images, the annealed samples are smoother than the unannealed samples. It is important to note that because there is no direct correspondence between the topography and transmission images, the contrast is not introduced by the variation in film

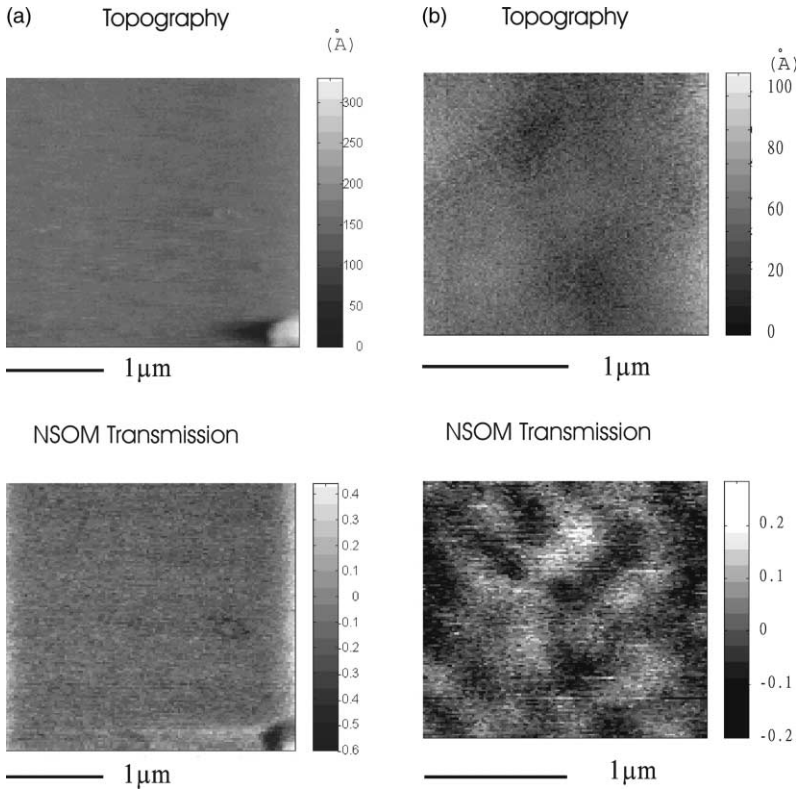

Fig. 5. The topography and NSOM transmission images of (a) pre-annealed and (b) annealed spin-cast samples.

thickness, but due to the difference in optical density at 543 nm. The lighter spots in NSOM image correspond to regions where aggregation is prevailing, while less aggregated chain segments are available in the relatively darker spots. This interpretation to the NSOM images is based on the absorption depicted in Fig. 4(a). Note that previous reported topographical images had been able to show that annealing modifies the film morphology by smoothening the surface topography [2,5]; however, there was no evidence for the formation of aggregated domains such as those shown in Fig. 5 [32]. Solvent might play important role for these different behaviors. The NSOM optical images show that the films have become less uniform upon annealing, the lower energy chains congregating in certain areas. If these chains are more close packed, then the chain in the other areas must be less close packed. Therefore, after annealing the interchain distance must have increased in some areas and decreased in other areas. This would be responsible for the off-diagonal disorder in the annealed TOF results.

Based on the results in Figs. 4 and 5, we propose that the observed transport phenomena are due to the enhancement of inhomogeneity in the annealed samples following the formation of nanometer scale domains. The decrease in mobility is due to (i) the increase in the distance between the larger energy gap chains outside the closely packed regions (this may act as a rate-limiting step in transport), (ii) an over-all increase in the level of off-diagonal disorder (large spread in the distribution of interchain distance), (iii) the smaller energy gap chains in the ordered regions acting as traps (effectively broadening the transport DOS width). As a result, the hopping of charge carriers is slowed down and the distribution of mobility values is also broadened, i.e. becoming more dispersive. The role of grain boundary between

amorphous and crystalline regions in the charge transport need further studies.

The present studies have implications on device performance. The enhancement of MEH-PPV based PLED performance through thermal annealing has been reported recently by Lee and Park [2] and Nguyen et al. [3]. Based on an ITO/MEH-PPV/Al device structure, it was demonstrated that annealing of the polymer layer, both before and after the deposition of Al electrode, improves the device behavior. From the view point of thermodynamics, annealing supplies the necessary energy to the polymer chains so that they can reorganize themselves towards forming lower energy structures. The formation of aggregation, whose PL quantum efficiency is much lower than single-chain species [27,28] is therefore expected to suppress the electroluminescence efficiency. However, they found that the overall device performance was actually improved. This was attributed to better polymer/cathode characteristics upon annealing. Better polymer/Al contact due to smoother polymer topography which facilitates the injection of electrons, an improvement that over-compensates the loss in PL efficiency. The present work provides further insights. The electron conduction in the PPV derivatives, including MEH-PPV, is smaller than the hole due to the presence of traps [29] or lower electron mobility [9]. As a result, the recombination zone is usually restricted to regions close to the cathode [30]. Unfortunately, the electroluminescence efficiency is then sacrificed due to non-radiative energy transfer from the excitons to the cathode. The region where electron and hole recombine is another key parameter that affects the device performance and this factor has been studied by recent work of Blom et al. [31]. As depicted in Fig. 3, annealing greatly lowers the hole mobility in the samples, and hence, the region of electron-hole pair recombination is expected to be shifted further away from the cathode. Consequently, the quenching due to cathode is reduced, which should also help to improve device quantum efficiency. Seemingly counter-intuitive at first sight, an optimum power efficiency in a PPV-based PLED was achieved by decreasing the hole mobility so that recombination does not take place near the cathode.

4. Conclusion

In summary, film morphology plays an important role in the charge transport in MEH-PPV films. Films prepared from toluene feature non-dispersive transport. The hole mobility at field 1.2×10^5 V/cm was determined as 9.8×10^{-6} cm^2/V s. Further processing by thermal annealing was found to alter the film morphology through the formation of aggregated grains, separated by the less aggregated domains. The observed transport phenomena are due to the enhancement of inhomogeneity in the annealed samples following the formation of nanometer scale domains. As a result, non-dispersive transport no longer exist in the post-annealed films. In addition, the hole mobility at 1.3×10^5 V/cm dropped down to 4.5×10^{-7} cm^2/V s, about one order of magnitude lower.

Acknowledgements

We gratefully acknowledge helpful comments by the reviewers. This research is supported by the Excellent Project, Education Ministry, Taiwan, ROC.

References

[1] J.H. Burroughes, D.D.C. Bradley, A.R. Brown, R.N. Marks, K. Mackey, R.H. Friend, P.L. Burn, A.B. Holmes, Nature 347 (1990) 539.
[2] T.-W. Lee, O.O. Park, Adv. Mater. 12 (2000) 801.
[3] T.-Q. Nguyen, R.C. Kwong, M.E. Thompson, B.J. Schwartz, Appl. Phys. Lett. 76 (2000) 2454.
[4] T.-Q. Nguyen, I.B. Martini, J. Liu, B.J. Schwartz, J. Phys. Chem. B 104 (2000) 237;
T.-Q. Nguyen, B.J. Schwartz, R.D. Schaller, J.C. Johnson, L.F. Lee, L.H. Haber, R.J. Saykally, J. Phys. Chem. B 105 (2001) 5153.
[5] T.-Q. Nguyen, V. Doan, B.J. Schwartz, J. Chem. Phys. 110 (1999) 4068.
[6] M. Gailberger, H. Bässler, Phys. Rev. B 44 (1991) 8643.
[7] H. Meyer, D. Haarer, N. Naarmann, H.H. Hörhold, Phys. Rev. B 52 (1995) 2587.
[8] P.W.M. Blom, M.J.M. de Jong, J.J.M. Vleggaar, Appl. Phys. Lett. 68 (1996) 3308.
[9] L. Bozano, S.A. Carter, J.C. Scott, G.G. Malliaras, P.J. Brock, Appl. Phys. Lett. 74 (1999) 1132.

[10] M. Redecker, D.D.C. Bradley, M. Inbasekaran, E.P. Woo, Appl. Phys. Lett. 73 (1998) 1565.
[11] D. Hertel, H. Bässler, U. Scherf, H.H. Hörhold, J. Chem. Phys. 110 (1999) 9214.
[12] C. Im, H. Bässler, H. Rost, H.H. Hörhold, J. Chem. Phys. 113 (2000) 3802.
[13] P.W.M. Blom, M.C.J.M. Vissenberg, Mater. Sci. Eng. R 27 (2000) 53.
[14] P.W.M. Blom, M.C.J.M. Vissenberg, Phys. Rev. Lett. 80 (1998) 3819.
[15] E. Lebedev, Th. Dittrich, V. Petrova-Koch, S. Karg, W. Brütting, Appl. Phys. Lett. 71 (1997) 2686.
[16] I.H. Campbell, D.L. Smith, C.J. Neef, J.P. Ferraris, Appl. Phys. Lett. 74 (1999) 2809.
[17] A.R. Inigo, C.H. Tan, W.S. Fann, Y.S. Huang, G.Y. Perng, S.A. Chen, Adv. Mater. 13 (2001) 504.
[18] P.K. Wei, J.H. Hsu, W.S. Fann, K.R. Chuang, H.T. Lee, S.A. Chen, Appl. Opt. 35 (1997) 3301.
[19] A.R. Inigo, Private communications.
[20] N.T. Harrison, G.R. Hayes, R.T. Phillips, R.H. Friend, Phys. Rev. Lett. 77 (1996) 1881.
[21] P.M. Borsenberger, E.H. Magin, M. Van der Auweraer, F.C. De Schryver, Phys. Status Solidi A 140 (1993) 9.
[22] Yu.N. Gartstein, E.M. Conwell, Chem. Phys. 245 (1995) 351.
[23] L.B. Schein, A. Peled, D. Glatz, J. Appl. Phys. 66 (1989) 686.
[24] W.G. Gill, J. Appl. Phys. 43 (1972) 5033.
[25] H. Bässler, Phys. Status Solidi B 175 (1993) 15.
[26] Y. Shi, J. Liu, Y. Yang, J. Appl. Phys. 87 (2000) 4254.
[27] M. Yan, L.J. Rothberg, E.W. Kwock, T.M. Miller, Phys. Rev. Lett. 75 (1995) 1992.
[28] R. Jakubiak, C.J. Collison, W.C. Wan, L.J. Rothberg, J. Phys. Chem. A 103 (1999) 2394.
[29] P.W.M. Blom, M.J.M. de Jong, J.J.M. Vleggaar, Appl. Phys. Lett. 68 (1996) 3308.
[30] G.G. Malliaras, J.C. Scott, J. Appl. Phys. 83 (1988) 5399.
[31] P.W.M. Blom, M.C.J.M. Vissenberg, J.N. Huiberts, H.C.F. Martens, H.F.M. Schoo, Appl. Phys. Lett. 77 (2000) 2057.
[32] T.-Q. Nguyen, B.J. Schwartz, R.D. Schaller, J.C. Johnson, L.F. Lee, L.H. Haber, R.J. Saykally, J. Phys. Chem. B 105 (2001) 5153.